Available online at www.sciencedirect.com
ScienceDirect
International Journal of Heat and Mass Transfer 51 (2008) 4249–4259
International Journal of HEAT and MASS TRANSFER
www.elsevier.com/locate/ijhmt

Visualization and performance measurement of operating mesh-wicked heat pipes

Shwin-Chung Wong *, Yi-Huan Kao [1]

Department of Power Mechanical Engineering, National Tsing Hua University, Hsin-Chu 300, Taiwan, ROC

Received 18 July 2007; received in revised form 18 December 2007
Available online 8 April 2008

Abstract

This work presents visualization of the evaporation/boiling process and thermal measurements of operating horizontal transparent heat pipes. The heat pipes consisted of a two-layered copper mesh wick consisting of 100 and/or 200 mesh screens, a glass tube and water as the working fluid. Experimental results indicated that nucleate boiling was prompted for a wick having a fine 200-mesh bottom layer. When the fluid charge approximately equaled the pore volume in the wick, the water–vapor interface receded into more curved menisci with increasing heat load Q. Thus, larger capillary forces and evaporation areas were attained to meet the increasing need of liquid supply and evaporation rate at the water–vapor interface. At $Q = 40$ and 45 W, the water film became less than 100 μm and the nucleate boiling observed at lower heat loads disappeared. Optimal thermal characteristics with smallest thermal resistances across the evaporator and lowest overall temperature distributions were found for such a wick/charge combination. Under a smaller charge, partial dry-out was observed in the evaporator. Under a larger charge, liquid recession with increasing heat load was limited and bubbles grew and burst violently at high heat loads. The effects of different wicks and fluid charges on the evaporation/boiling characteristics were discussed.

Keywords: Heat pipe; Evaporation; Nucleate boiling; Two-phase heat transfer

1. Introduction

The heat pipe has been widely applied for cooling and heat spreading applications due to its superior heat conductivity. It utilizes the large latent heat associated with phase change. At its evaporation section (evaporator), the heat from the heat source, such as a CPU of a computer, is absorbed by the working liquid via evaporation. The vapor condenses at a distant location to release the latent heat. The condensed liquid is then drawn back to the evaporator by the capillary force therein to complete a thermal cycle. A good heat pipe is characterized by a low thermal resistance and a high dry-out tolerance. The most important factor is related to the characteristics of the evaporator. The type, thickness, porosity and structure of the wick, and even the contact condition between the wick the container wall, all more or less affect the performance of the evaporator [1–3]. The evaporation/boiling process in the heat pipe wick is different from that for the extensively-studied pool boiling associated with a wick-covered wall in that liquid–vapor interfacial menisci normally exist in the wick. The menisci are related to the area for evaporation as well as the capillary returning force for the working fluid. Faghri [1] qualitatively described the recession process of the liquid layer as well as the likely evaporation/boiling transition with increasing heat flux. At a low heat flux, the heat transfer across the wick is basically by conduction and convection, without boiling. Menisci form by the capillary effect at the solid–liquid–vapor interface. As the heat flux is increased, the menisci recede into the wick due to intensified evaporation. Nucleate boiling occurs at the heated wall or even the wick surface for a further increased heat flux. Bubbles grow, escape

* Corresponding author. Tel.: +886 3 571513x33749; fax: +886 3 5722840.
E-mail address: scwong@pme.nthu.edu.tw (S.-C. Wong).
[1] Undergraduate student.

0017-9310/$ - see front matter © 2008 Elsevier Ltd. All rights reserved.
doi:10.1016/j.ijheatmasstransfer.2008.01.022

to the liquid surface and burst rapidly. The bubbles in the wick may block the liquid return and the bubble bursting may disrupt the menisci to reduce the capillary force for liquid circulation. At an even further heat flux, rapidly-growing bubbles coalesce before they can escape through the wick structure, leading to the film boiling. As a result, the heat pipe wall temperature increases rapidly and a heat transfer limit may be reached. Mughal and Plumb [2] experimented on an open flat heat pipe with R-11 as the working fluid. The evaporator was made of thick (4.76 mm or 3.18 mm) copper foametal. The copper plate temperatures beneath the evaporator were measured against heat flux. The variation of heat flux versus the superheat of the copper plate showed a transition from larger slopes at low superheats to smaller slopes at higher superheats. If several channels were cut in the evaporator wick, the transition was sustained to a larger heat flux while at a lower superheat. It was suggested that the channels in the wick helped vapor escape. Consequently, the nucleate boiling extended to a larger heat flux before transiting to the film boiling with a vapor film blanketing the evaporator surface. Brautsch and Kew [3] visualized the heat transfer processes of a vertical aluminum heater surface covered with stainless steel meshes capillarily wetted by distilled water. At a low heat flux, small bubbles formed first on the heater surface and then in the mesh wick. The bubbles could leave without being trapped by the mesh. As the heat flux was increased, bubbles coalesced into vapor patches which insulated the heater surface from water and led to intermittent local dry-out. Intermittent bursting of vapor patches was observed. The bubbles in the wick and the bursts impeded the liquid return and the heat transfer process. Also found was that while the maximum attainable heat flux increased with wick thickness, the heat transfer coefficient decreased, as a thick wick presented a wider path for liquid return but a larger thermal resistance for heat transfer across the wick. Li et al. [4,5] measured the heat transfer coefficients and the critical heat fluxes (CHF) associated with the evaporation/boiling process for a horizontal copper surface sintered with multiple layers of copper mesh. The total wick thicknesses were thinner than 0.8 mm. The water level was fixed at the top of the mesh wick before heating. With the contact resistance for the copper plate and the mesh wires minimized by careful sintering, very high heat transfer coefficients and CHFs were obtained. As the heat flux was increased, the variation of the evaporation/boiling behavior basically followed the above-mentioned description of Faghri [1]. But Li et al. [4,5] further indicated that the liquid surface receded non-uniformly at a large heat flux with the lowest point at the center of the heated area. When the liquid thickness around the central area became very thin, the effective thin film evaporation is dominant. If the heat flux continued to increase, initial dry-out appeared at the center of the heated area. Since nucleate boiling was suppressed in the thin film evaporation situation, the ultimate heat transfer limit would be the capillary limit, rather than the boiling limit. Their measurements also indicated a sharp drop in wall temperature upon transition from the conduction/evaporation mode to nucleate boiling. The heat transfer coefficient increased with increasing heat flux in the nucleate boiling and the thin liquid film evaporation regimes until the occurrence of partial dry-out. The effects of wick thickness, mesh size and wick porosity on the heat transfer coefficient and CHF were also investigated.

Another important parameter is the working fluid charge in the heat pipe. Although it is a common practice that optimal fluid charge is slightly more than that needed to saturate the wick pores, the fundamental studied on the effects of liquid amount on the evaporation/boiling process in a heat pipe is lacking, to the knowledge of the authors.

Above all, the visualization of the evaporation/boiling process in the evaporator of an operating heat pipe is not available in the literature due to experimental difficulties. With proper temperature measurements, such studies can provide deeper insights for the complicated processes in two-phase heat transfer devices. This is what this study aims for. By developing a technique to fabricate transparent heat pipes and measure the internal vapor temperature at the evaporation section, the visualized evaporation/boiling behavior at the evaporator can be correlated with the thermal characteristics. The effects of wick mesh size and fluid charge on the evaporation/boiling process and the heat-pipe performance at different heat loads will be investigated.

2. Experimental methods

2.1. Test setup

The test setup is shown in Fig. 1. A transparent heat pipe having two layers of copper mesh as the wick and distilled water as the working fluid was tested horizontally at different working fluid charges and heat loads. The length of the heat pipes was 15 cm and the outer diameter was 6 mm. The 3-cm long evaporation section was attached on a copper heating plate on top of a well-insulated electric heater. The middle 9-cm adiabatic section was tightly wrapped with ceramic insulator. The final 3-cm long condensation section was cooled with a constant-temperature water jacket (water temperature of 15 ° C and flow rate of 25 ml/s). Temperatures measured at four points are denoted by $T1$–$T4$, respectively. A thermocouple was attached to the first measuring point ($T1$) at the side wall of the heating plate right under the heat pipe end. Another bare thermocouple penetrated the heat pipe wall to measure the internal vapor temperature above the evaporator ($T2$). Two other thermocouples measured the outer wall temperatures of the adiabatic section ($T3$ and $T4$) under the ceramic insulator. The thermocouple beads were attached to the glass tube with a small amount of conductive paste. They were, respectively, located at 6 cm and 9 cm from the evaporator end of the heat pipe. Readings of all the thermocouples, of K type with a 0.25 mm wire

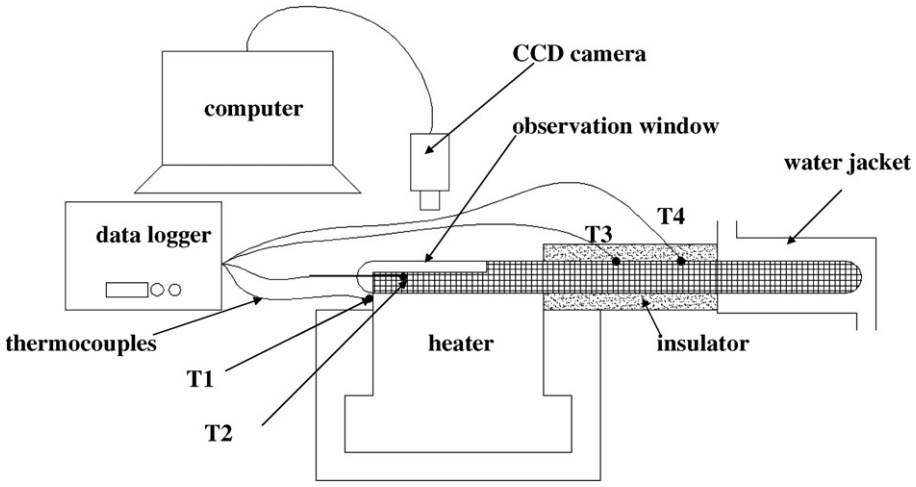

Fig. 1. Test setup.

diameter (Omega, Inc.), were recorded by a data logger (Fluke, Hydra Series II) with a resolution of 0.1 °C. A slender observation window was made by cutting off a ceiling portion of the wick at the evaporation section. A CCD camera equipped with a microscopic lens (Optem, Zoom 125), shooting vertically downward through the observation window, recorded the evaporation/boiling process in the evaporator at a framing rate of 30 fps. Illumination was provided by a high-intensity zenon light (Zolix, LHX150).

Fig. 2 shows the cross-sectional view of the arrangement of the heat pipe on the heater. The lower half of the heat pipe was connected to a semi-cylindrical trench on top of the copper plate via a thin layer of thermal interface material (TIM, Dow Corning TC5021 thermal paste, having a thermal conductivity of about 3 W/m K). The bottom surface of the copper plate (3 cm × 3 cm) was connected to the uniform-temperature top surface (3 cm × 3 cm) of a long heating rod via another layer of TIM. The heating rod, electrically heated in its base with cartridge heaters, was enclosed in a bakelite box stuffed with ceramic insulating material except for its top end. The evaporation section of the heat pipe and the heating plate were insulated within a cap made of bakelite and ceramic insulating material. During a test, the long opening of the cap was covered with a thick layer of ceramic insulator until a steady state was reached, defined as when every temperature reading varied by less than 0.5 °C in 10 min. For video recording, the thick ceramic insulator would be removed for less than 30 s to avoid the effect of heat loss. The nominal heat load Q was determined by the current and voltage readings of the DC power supply which powered the cartridge heaters. No estimation of the heat loss to the environment from the heater was made. This is not critical for the present study since only the relative amounts of Q are important.

2.2. Fabrication of heat pipe

The glass tube, 6 mm OD and 5 mm ID, was cleaned with acetone and rinsed with water. Copper wire meshes were cleaned with acetone and then diluted nitric acid solution, before water rinsing. All the cleaning processes were

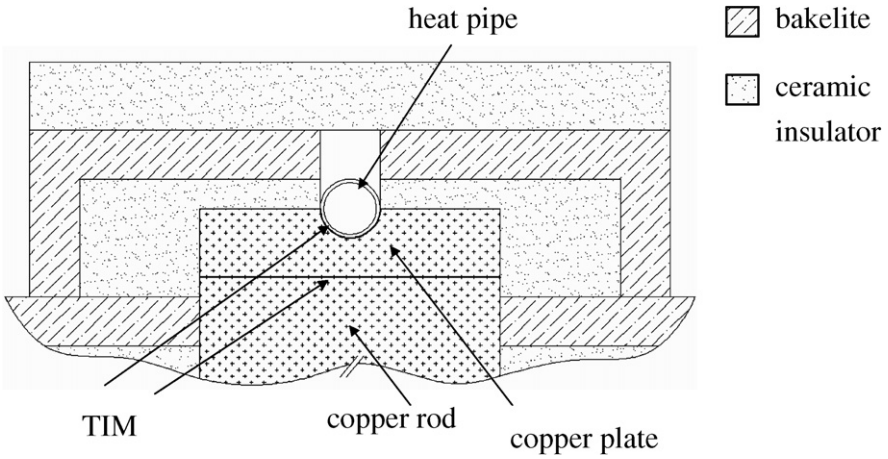

Fig. 2. Cross-sectional view of the arrangement of heat pipe on the heater.

conducted in an ultrasonic cleaning tank. Into one end of the glass tube was inserted a bare thermocouple (K type, Omega, Inc.) for $T2$ measurement. The tube end was then melted with a torch to form a thermocouple-penetrated closed end. A small amount of silica was applied on this closed end to avoid air leakage through the thermocouple–glass interface. Through the other tube end were then inserted the cleaned copper wire mesh, with a slender opening at the evaporation section as the observation window. With its restoring force, the wire mesh could contact closely with the inner surface of the glass tube. A suitable amount of high-purity distilled water was then filled in the tube right before the evacuation of non-condensable gases through the open end using a vacuum pump. Finally, the open end was melted and closed to form a heat pipe.

2.3. Experimental parameters

Parameters considered in this study included fluid charge, heat load and wick structure.

Wicks investigated included a two-layer 100 mesh wick and a wick consisting of a layer of 200 mesh screen covered with another layer of 100 mesh screen. The 100 mesh screen has a wire diameter of 0.114 mm and a wire spacing of 0.14 mm; the 200 mesh screen has a wire diameter of 0.055 mm and a wire spacing of 0.07 mm. The wick thicknesses were, respectively, 0.42 mm and 0.33 mm. The porosities of both wicks were estimated to be about 0.65, according to the single-layer formula for mesh screen from ESDU [6]. We also studied a two-layer 100 mesh screen with its lower layer at the evaporation section sintered with a small amount of irregular-shaped copper particles, as shown in Fig. 3.

The fluid charge was rated based on the void volume in the wick. Three different fluid charges were selected: 80%, 100% and 120% charge. The 100% charge is defined as

$$100\%\ \text{charge} = \text{Vol} \times \varepsilon$$

where Vol is the total volume of the wick and ε is the porosity of the wick. However, the actual fluid charge was slightly different from the nominal value in each test. Generally the differences were controlled within ±6%.

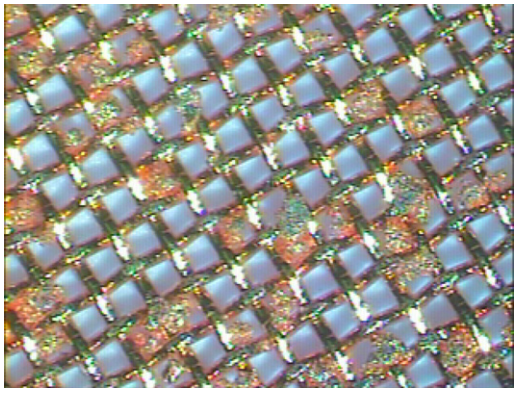

Fig. 3. A 100 mesh screen sintered with irregular-shaped copper particles.

The heat load was increased stepwise from 20 W to 45 W with an increment of 5 W. For each heat load, steady state must be reached before temperature measurements and recordings were taken.

3. Results and discussion

3.1. Evaporation/boiling process in 2 × 100 mesh wick

The evaporation/boiling processes in operating heat pipes were first investigated for a wick having two layers of 100 mesh screen at 80% and 100% water charges, respectively. The temperature and the flow rate of the cooling water were fixed.

3.1.1. 80% fluid charge

Under an 80% fluid charge, the water level was relatively high when the heat load Q was 20 W and 25 W, as shown in Fig. 4a and b. Only individual peaks of the upper mesh wires were exposed, identified by their very bright reflection. The relatively high water level was partly because of the insufficient capillary force of the coarse mesh to fully hold water against gravity. More water was present at the bottom portion than in the upper portion. In Fig. 4a, the menisci at 20 W were less concave, as the wire diameter in the image of the lower mesh was reduced to a limited extent. When Q was increased to 25 W, the water surface receded slightly further to form more concave menisci, as evidenced by the significant reduction of the wire size in the lower mesh image (see Fig. 4b and Video 1 in the online version of this article). The more curved menisci not only generated a larger capillary force to draw more liquid into the evaporator, but increased the evaporation surface. In addition, the evaporation temperature would also increase (cf. Fig. 6). Similar, but stronger, adjustment in the water surface and evaporation temperature extended to $Q = 35$ W. At these heat loads the evaporation process appeared quiet without nucleation. At $Q = 40$ W, however, nucleate boiling appeared, as shown in Video 2 in the online version of this article. Large bubbles under the lower mesh were observed to repeatedly grow and shrink after a burst. The inner surface of the top observation window was frequently blurred by erupted water drops. In Fig. 5a, under the lower mesh existed a large bubble which somehow raised the water surface into less concave menisci. After a burst, the bubble shrank considerably and the menisci, except at a small left portion of the photo, turned more concave, as shown in Fig. 5b. Shortly afterward, the bubble grew and the region of less concave menisci expanded to the right (Fig. 5c and d) before next burst. Such repeated sequences did not have stable periods, ranging from less than a second to a few seconds. As Q was further increased to 45 W, strong boiling still prevailed as evidenced by the frequent collisions of the erupted water drops on the observation window. It is noted that the

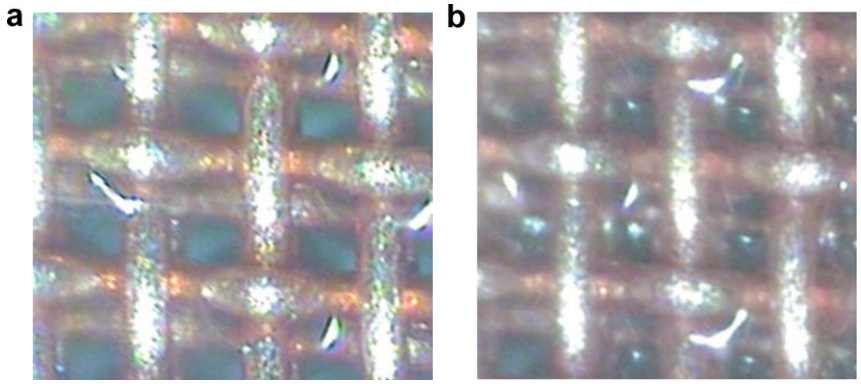

Fig. 4. Different images of the evaporator due to different menisci, 80% fluid charge (wick: 2 × 100 mesh): (a) $Q = 20$ W, less concave meniscus and (b) $Q = 25$ W, more concave meniscus.

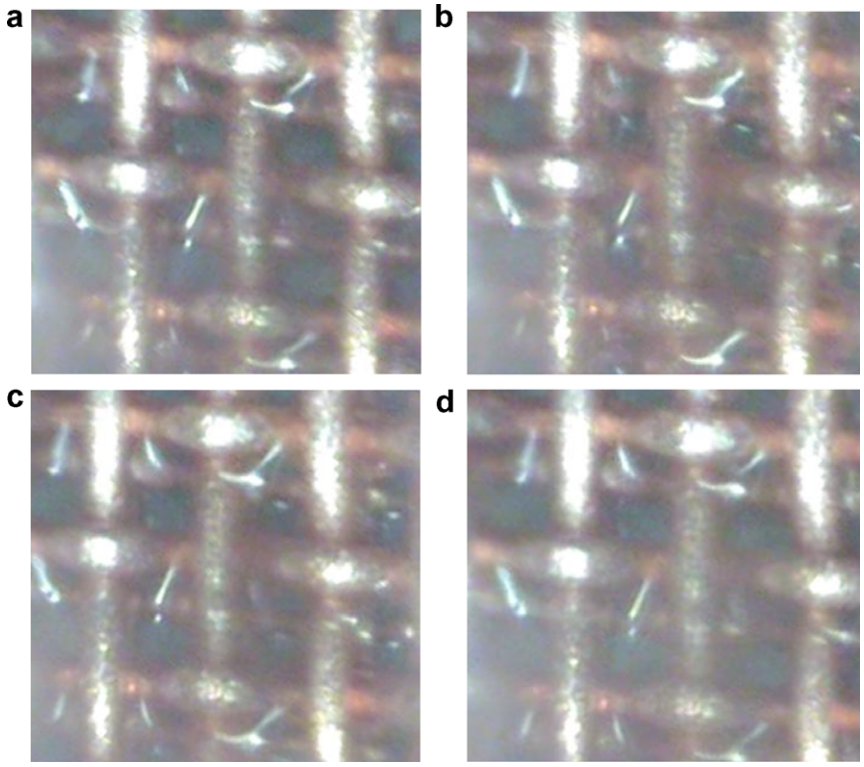

Fig. 5. Sequential images showing activities of a large bubble; $Q = 40$ W, 80% fluid charge (wick: 2 × 100 mesh): (a) bubble formed, (b) bubble partially shrunk after a burst, (c) bubble regrowing and (d) bubble formed prior to another burst and shrinking.

two-layer mesh wick in this study was not sintered together and the effective thermal conductivity across the wick could be relatively low. Significant superheat at the wick bottom was expected so that nucleate boiling could be activated as a result. This finding does not necessarily apply to thin sintered wicks for which superheat at the wick bottom may be insufficient to activate boiling.

3.1.2. 100% fluid charge

Under a 100% fluid charge, the water level at the bottom region of the evaporation section was higher than for the 80% charge with slightly smaller exposed peak regions. At $Q = 20$–25 W, the water surface was also rather quiet. At $Q = 30$ W, the water surface appeared agitated and the observation window was occasionally hit by water drops. These reflected mild boiling activity. At $Q = 35$ W, stronger boiling led to frequent drop collisions on the observation window. It is noted that under an 80% charge boiling was not observed until $Q = 40$ W. The earlier inception of boiling at a larger charge may be attributed to the larger wall superheat associated with the larger water/wick thickness. At higher heat loads, $Q = 40$ or 45 W, the evaporation/boiling behavior was similar except that the drop collision frequency appeared higher. Video 3 in the online version shows the evaporation/boiling behavior at $Q = 40$ W. A number of bubbles can be seen to anchor at

the intersections of the upper mesh layer. The shivering of the water surface should result from the eruptions of these bubbles. It is not clear whether these bubbles are isolated ones or the protruding parts of larger bubbles underneath.

3.1.3. Effects of fluid charge

Fig. 6 compares the temperatures at various locations under different heat loads for nominal 80% and 100% charges, respectively. In the figure, each temperature datum represents an average of three runs, with the upper and lower uncertainty bar, respectively, representing the highest and lowest reading of the three tests. The large values of $T1$, representing the heating surface temperature, resulted from the high thermal resistance of the glass wall. Nonetheless, the temperature difference ($T1$–$T2$) can reflect the thermal resistance of the evaporator, as the thermal resistances of glass wall and TIM were unchanged. In Fig. 6, it can be seen that while $T2$–$T4$ are similar for both charges, the values of $T1$ for the 80%-charge cases are significantly lower. The similarity between $T2$–$T4$ can be understood in that the thermal resistances between $T2$ and the cooling water were approximately the same, although the water film at the condenser should be thicker for the 100% charge. The significant differences between the values of $T1$ reflect the differences of the thermal resistance across the evaporator. Since the water levels in the evaporator were higher for the 100% charge, larger thermal resistances and hence higher heating surface temperatures $T1$ were expected.

3.2. Evaporation/boiling process in 100 + 200 mesh wick

3.2.1. 100% charge

When the 200 mesh screen (wire diameter of 0.055 mm and wire spacing of 0.07 mm, half of those of the 100 mesh screen) was adopted as the lower layer of the wick, nucleate boiling occurred at a much smaller heat load than for the 2 × 100 mesh wick. Fig. 7 illustrates two sequential images showing the escape of a bubble from the evaporator with a 200 mesh lower layer at $Q = 20$ W. The images were taken

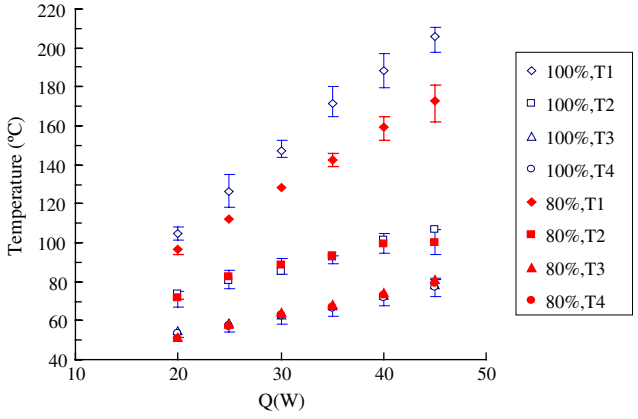

Fig. 6. Temperature distributions at different locations ($T1$: heating surface, $T2$: above evaporator, $T3$, $T4$: adiabatic section) under different water charges and heat loads (wick: 2 × 100 mesh).

in the end half, about 0.5–1.5 cm from the heat pipe end, of the 3-cm long evaporation section. In Fig. 7a, the menisci at the lower left region have been raised so that the size reduction for the lower mesh wires was less than for other regions. In Fig. 7b, the bubble has escaped and the image reduction becomes uniform. The process is shown in Video 4 in the online version of this article, in which a relatively large bubble can be seen between the two mesh layers. It lasted for at least 6 s before escape by a burst. It can also be seen that nucleate boiling was not frequent for $Q = 20$ W. As indicated earlier, nucleate boiling appeared at larger heat loads for the 2 × 100 mesh wick. This is because the fine 200 mesh screen provided more nucleation sites for boiling. In the front half of the evaporator, 1.5–2.5 cm from the heat pipe end, nucleate boiling was not observed and the situation was rather quiet (see Video 5 in the online version of this article). The water level was slightly higher at this region, judged by the less size reduction for the submerged mesh wires. The non-uniform liquid level in the evaporator has been explained by Li and Peterson [5] using a simple analysis based on mass and energy conservation.

For $Q = 25$ W, nucleate boiling was still observed in the end-half evaporator. But now the relatively large bubbles as seen for $Q = 20$ W were not observed. Instead, a large number of small bubbles in the wick were seen to grow and burst (see Video 6 in the online version). With further water level recession, the menisci became more curved, as shown in Fig. 8a. Except for slight local agitation of the water surface upon bubble bursting, the situation in the evaporator appeared rather stable. Again, the situation in the front-half evaporator was quiet, without nucleate boiling (see Video 7 in the online version). Also, the water level was higher than that in the end-half region. The results for $Q = 30$ W were essentially similar for the end-half evaporator, as shown in Video 8 in the online version. At $Q = 35$ W, weak nucleate boiling could also be observed in the front-half region.

When Q was increased to 40 W or 45 W, an interesting phenomenon happened: the nucleate boiling disappeared and the situation in the whole evaporator appeared very quiet. Videos 9 and 10 in the online version, respectively, show the evaporation processes in the end half and front half of the evaporator at 45 W. Fig. 8b shows that the water level in the end half has receded to the lower 200 mesh layer, with its peaks exposed. The averaged water thickness is less than 100 μm since the thickness of the 200 mesh screen is 110 μm. In addition, the area of the water–vapor interface can be larger with a larger number of concave menisci. These favorable conditions help reduce the thermal resistance across the evaporator. It will be shown later that the combination of 100 + 200 mesh wick and 100% charge presents the optimal thermal characteristics among other combinations of wick type and fluid charge tested in the present study.

In a couple of tests, the heat load was raised to 50 W without reaching the heat transfer limit.

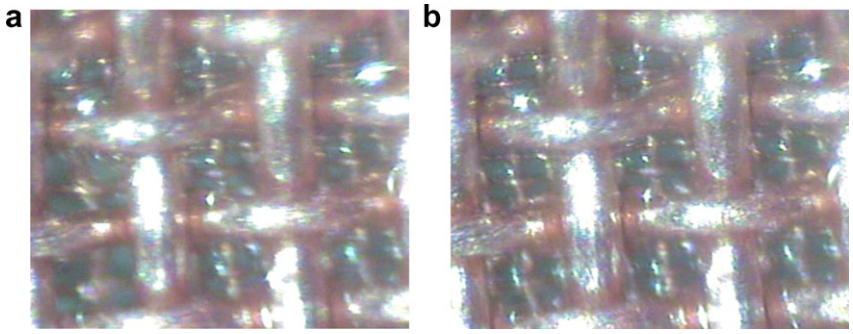

Fig. 7. Sequential images showing escape of a bubble at the end half of the evaporator at $Q = 20$ W with 100 + 200 mesh wick and 100% charge: (a) before escape and (b) after escape.

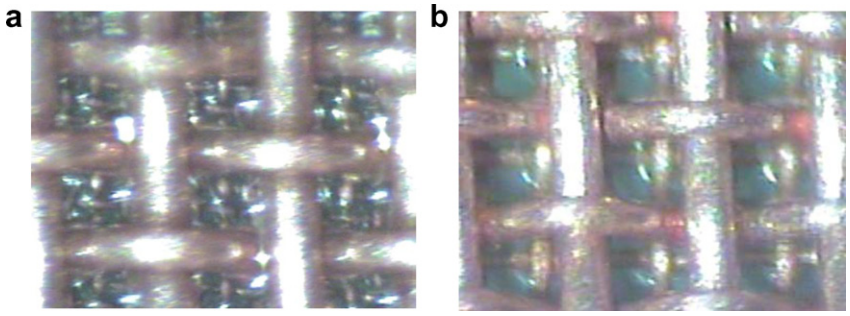

Fig. 8. Images at the end half of the evaporator with 100 + 200 mesh wick and 100% charge: (a) $Q = 25$ W and (b) $Q = 45$ W.

3.2.2. 80% charge

Under 80% charge, the water level in the evaporator was relatively low. At $Q = 20$ W, the water level at the end half was so low that the bottom fine wires were mostly exposed. In the front half the water level was higher, somewhat above the lower layer. At this test condition, very sparse and slow nucleate boiling was observed. At $Q = 25$ W, the end half of the evaporator has completely dried out, as shown in Fig. 9a. Moving to the middle part of the evaporator, the margin of the water can be identified. In Fig. 9b, the left region was dry but in the right region the lower mesh layer was wetted. The evaporation process was very quiet, without nucleate boiling. Similar evaporation behavior was observed for $Q = 30$–40 W, except for an expanded dry-out region. In these cases, dry-out was not preceded by nucleate boiling which had been suppressed at such a thin water layer condition.

The temperature distributions associated with the 100% and 80% charges are compared in Fig. 10. It can be seen that the temperatures above the evaporator and at the adiabatic section are slightly lower for the 100% charge by about 3–5 °C. But the differences of the heating surface temperatures are significant, which clearly resulted from the partial dry-out in the evaporator under the 80% charge. No measurement was made beyond $Q = 40$ W under the 80% charge because the heating surface temperature was too high.

Under 80% and 100% charges, the heat transfer limit was dominated by the capillary limit as nucleate boiling had been suppressed in the thin water film present before dry-out. In the experiments of Li and Peterson [5] on evaporation/boiling in mesh wick in an open environment, the capillary limit was found to be dominating because nucleate boiling was suppressed in the thin water film before dry-out.

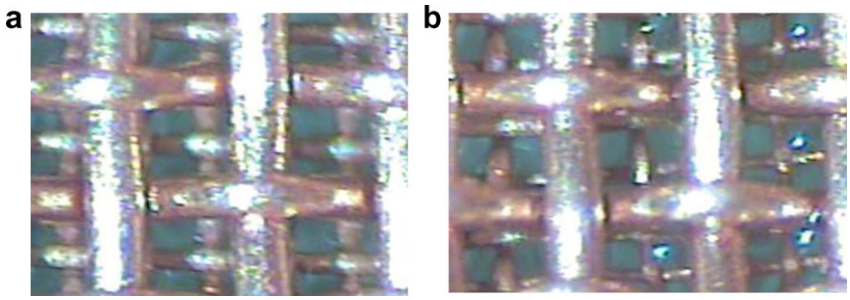

Fig. 9. Images of the evaporator at $Q = 25$ W with 100 + 200 mesh wick and 80% charge: (a) at the end half and (b) at a middle part.

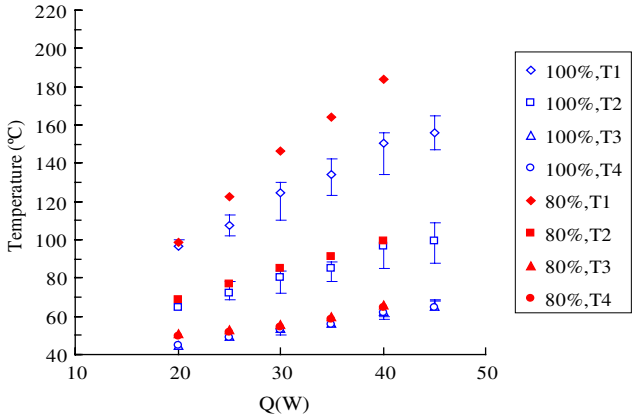

Fig. 10. Comparison of temperature distributions under 100% and 80% charges with the same 100 + 200 mesh wick ($T1$: heater surface, $T2$: above evaporator, $T3$ and $T4$: adiabatic section).

3.2.3. 120% charge

Under a 120% charge, the evaporator was mostly immersed in the water, especially at low heat loads. At $Q = 20$ W, nucleation could hardly be observed. But at $Q = 25$ W, bubble growth and burst could be observed (see Video 11 in the online version of this article). Fig. 11 shows the dynamic process of growth and burst of a large bubble trapped in the evaporator. With increasing heat loads, the boiling became more and more violent. Videos 12 and 13 in the online version, respectively, show the evaporation/boiling process in the end half and front half of the evaporator at $Q = 45$ W. In the end half, frequent and intense bubble bursting strongly agitated the water surface and the observation window was frequently hit by erupted water drops. The cycles of bubble growth and burst were rather rapid with efficient bubble escape. Also, the returning liquid flow did not seem to be blocked by the bubbles in the wick. In the front-half evaporator, no nucleate boiling was observed (see Video 13 in the online version). The high water level oscillated as a result of bubble activities in the end half. In a few cases, we attempted to raise the heat load up to 60 W. The heat transfer limit was not yet attained, while the vapor temperature above the evaporator had reached about 140 °C. However, the film-boiling limit could be more likely for such high-charge conditions.

The temperature distributions associated with the 100% and 120% charges are compared in Fig. 12. In general, the differences are insignificant except for $Q = 45$ W, while the evaporation/boiling mechanisms were very different. Under a 100% charge, the water–vapor interface receded to the lower fine mesh layer at $Q = 45$ W. Due to the large capillary force provided by the menisci within the fine mesh pores, the large amount of liquid needed at the high heat load could be supplied through the thin water film. Also, the total evaporation area was larger because of the larger number of concave menisci. The large area yielded a large evaporation rate without excessively raising the evaporation temperature. Furthermore, the average water thickness was smaller than 100 μm, leading to a smaller thermal resistance across the evaporator. This kept the superheat of the wall or the bottom mesh wires below the inception superheat of nucleate boiling. Another possible heat dissipation route at this situation was through the thin film evaporation. At the water–solid–vapor interface, there existed a very thin capillary layer with a very high evaporation coefficient [4,5]. Since the bottom mesh wires had a

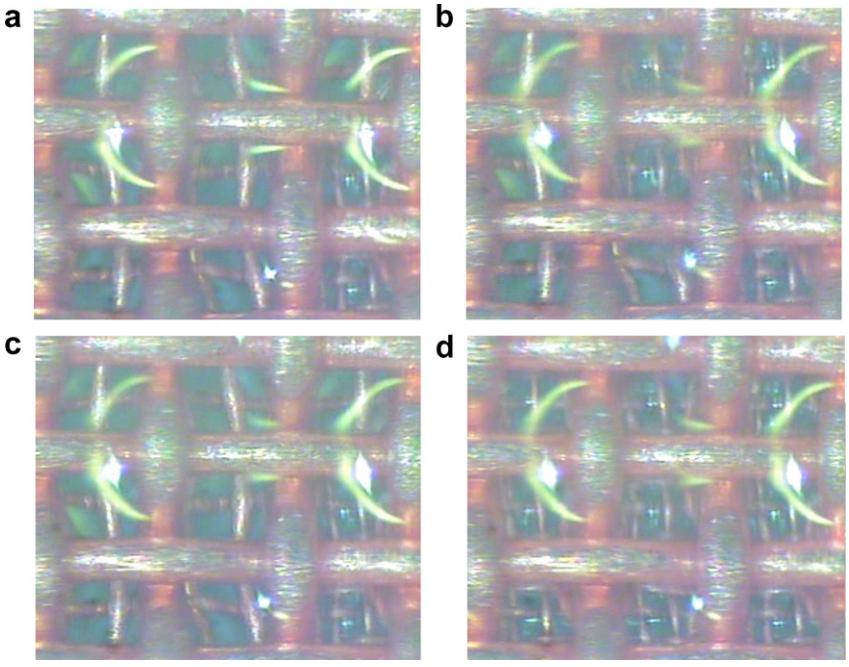

Fig. 11. Sequential images showing activities of a large bubble at $Q = 25$ W with 100 + 200 mesh wick and 120% charge: (a) bubble formed, (b) bubble partially shrunk after a burst, (c) bubble regrowing and (d) bubble shrunk after another burst.

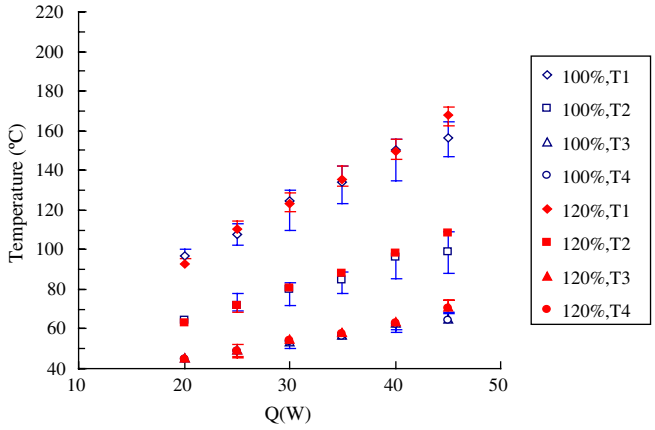

Fig. 12. Comparison of temperature distributions under 100% and 120% charges with the same 100 + 200 mesh wick.

higher temperature, the thin film evaporation could be more prominent at this low-water-level situation. Li and Peterson [5] also found that the best thermal performance was associated with the thin water film prior to dry-out. Their unloaded water level was fixed at the top of the mesh wick, similar to our 100%-charge conditions. Therefore, their results agree with our results under a 100% charge or less. However, our study on operating horizontal heat pipes further indicated that the heat transfer limit under a larger-than-saturation charge was more likely the film-boiling limit.

At lower heat loads, the water recession was limited and the menisci were formed within the upper coarse mesh. Hence, the evaporation area was not as large as at 45 W. The thermal resistance across the evaporator also was not as small. Therefore, at $Q = 20$–35 W, nucleate boiling occurred, leading to increased evaporation area and enhanced heat convection to cope with the heat load. Such evaporation/boiling characteristics were similar to those at the 120% charge, although the water thicknesses at equal heat loads were slightly thinner for the 100% charge. Consequently, the thermal characteristics at lower heat loads were quite similar for both water charges.

At high heat loads, such as 40 or 45 W, not only the water thickness but the evaporation/boiling characteristics became very different for the two different charges. However, the temperature differences $T1$–$T2$ were still rather similar. In other words, under the 120% charge the thermal resistance across the thicker wick/water layer was similar to that across the very thin, boiling-free water film under the 100% charge. This can be attributed to the fact that the thermal resistance in the thicker wick/water layer was reduced by the boiling-enhanced convection.

3.3. Effects of different wicks

3.3.1. 100 + 200 and 2 × 100 mesh wicks

Fig. 13 compares the temperature distributions for the 100 + 200 mesh wick against those for the 2 × 100 mesh wick, both under the 100% charge. The temperature distributions for the 100 + 200 mesh wick were significantly lower at all heat loads, especially for the heating surface temperature. The first reason is that nucleate boiling occurred earlier in the 100 + 200 mesh wick with more nucleation sites in the lower 200 mesh wick. Nucleate boiling was observed at $Q = 20$ W for the 100 + 200 mesh wick, while not until $Q = 30$–35 W could boiling be observed for the 2 × 200 mesh wick. The second reason is related to the smaller thermal resistance for the thinner wick.

Fig. 14 compares the temperature distributions for the 100 + 200 mesh wick under the 100% charge against those for the 2 × 100 mesh wick under the 80% charge. It happened that the fluid charges were similar in these two conditions. In general, the thermal characteristics of the cases with the 100 + 200 mesh wick were still significantly better. Better thermal characteristics have been shown for the 2 × 100 mesh wick under the 80% charge than those under the 100% charge, especially for the thermal resistance across the evaporator. Since there were less nucleation sites in the 2 × 100 mesh wick, nucleate boiling was not observed until $Q = 40$ W for the 80% charge. As the heat load increased from 20 to 35 W, the menisci became more curved with the receding water surface. A larger evaporation area was thus provided to cope with the increasing heat load. However, without nucleate boiling, the evaporation temperatures were slightly higher for the 2 × 100 mesh wick, as shown in Fig. 14.

3.3.2. Effects of additional irregular-shaped particles

We also examined the evaporation/boiling process under a 100% charge when a small amount of irregular copper particles was sintered in the lower 100 mesh screen at the evaporation section (Fig. 3). No nucleate boiling was found below 30 W. At $Q = 35$ W, a number of very small bubbles were seen to grow and burst rapidly, as shown in Video 14 in the online version of this article. At

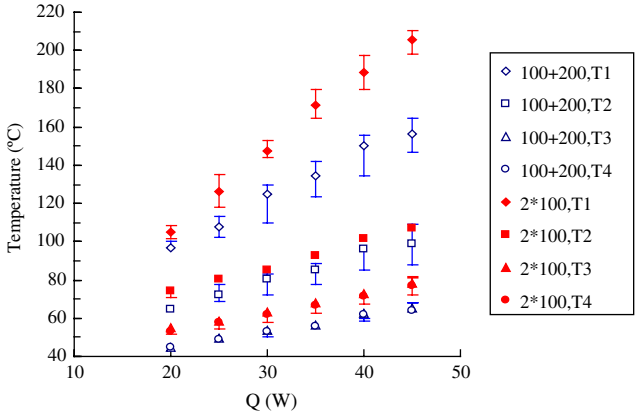

Fig. 13. Comparison of temperature distributions with 100 + 200 mesh wick and 2 × 100 mesh wick under 100% charge.

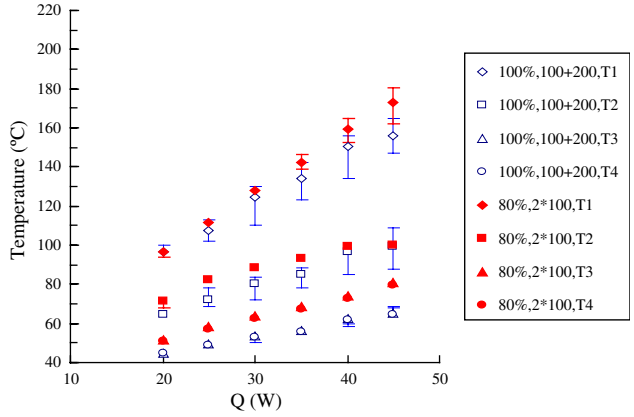

Fig. 14. Comparison of temperature distributions with 100 + 200 mesh wick under 100% charge and 2 × 100 mesh wick under 80% charge.

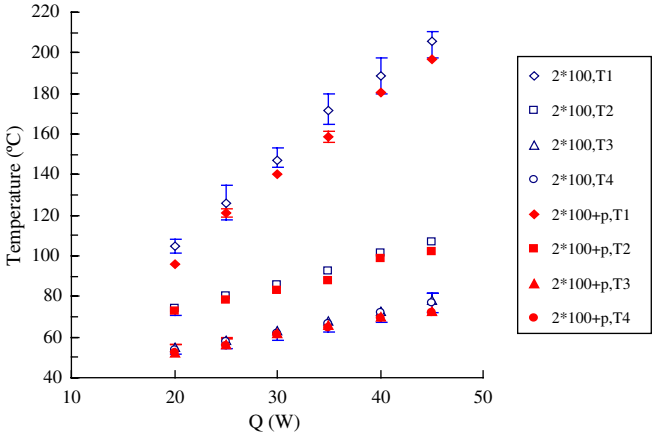

Fig. 15. Comparison of temperature distributions with and without irregular-shaped copper particles in the 2 × 100 mesh wick under 100% charge.

$Q = 40$ W, violent boiling with rapid bubble growth and strong bursting was observed (see Video 15 in the online version). Although the images were too fluctuating for unequivocal affirmation of its relationship with these particles, the boiling activity appeared significantly stronger than for the 2 × 100 mesh wick under similar conditions (cf. Video 3 in the online version). Fig. 15 shows that the thermal characteristics with the particles are slightly better than those without particles.

4. Conclusions

An experimental method was developed to enable simultaneously visualization and temperature measurement for the evaporation/boiling processes in the evaporator of operating horizontal heat pipes. By experimenting on different mesh wicks at different fluid charges and heat loads under steady-state conditions, the following conclusions were reached:

1. With the coarse mesh wick, nucleate boiling was absent at low heat loads and the heat was dissipated by surface evaporation on the water–vapor menisci within the mesh wires. Along with increasing heat load, the water–vapor interface receded into more curved menisci to provide a larger area for evaporation and capillary force for liquid supply. Nucleate boiling with large bubbles growing and bursting repeatedly occurred at a heat load larger than 30–40 W. Earlier inception of boiling occurred at a larger fluid charge, which may be attributed to the larger wall superheat associated with the larger water/wick thickness.
2. The fine mesh wick prompted the onset of nucleate boiling by providing more nucleation sites and consequently reduced the evaporation temperature.
3. The optimal thermal characteristics pertained to a combination of a fine bottom mesh layer and a fluid charge approximately saturating the wick. Under such conditions, the water–vapor interface receded with increasing heat load. Eventually, at large heat loads a thin water film with a large number of menisci could be sustained in the fine mesh pores by the strong capillary force therein. Due to the large evaporation area, small thermal resistance across the evaporator, and the possible contribution of thin film evaporation at the water–vapor–wire interface, both the evaporation temperature and the heating surface temperature were lowest among all the tested wick/charge combinations. In addition, nucleate boiling diminished and the evaporation process appeared very quiet.
4. With a smaller-than-saturation charge and a wick having a fine-mesh bottom layer, partial dry-out was observed in the evaporator and the heating surface temperatures became excessively high. The heat transfer limit was the capillary limit.
5. With a larger-than-saturation charge and a wick having a fine-mesh bottom layer, the water level recession was limited even at a large heat load. Nucleate boiling grew more violently with increasing heat load and bubbles could escape efficiently at $Q = 45$ W. The heat transfer limit was not reached up to $Q = 60$ W.
6. The irregular-shaped particles added in the coarse mesh wick appeared to promote nucleateboiling.

Acknowledgements

We are thankful to Professor Cheng-Huan Chen of the Department of PME, NTHU for kindly offering us the Xenon light.

Appendix A. Supplementary material

Supplementary data associated with this article can be found, in the online version, at doi:10.1016/j.ijheatmasstransfer. 2008.01.022.

References

[1] A. Faghri, Heat Pipe Science and Technology, Taylor & Francis, London, 1995.
[2] M.P. Mughal, O.A. Plumb, An experimental study of boiling on a wicked surface, Int. J. Heat Mass Transfer 39 (1996) 771–777.
[3] A. Brautsch, P.A. Kew, Examination and visualization of heat transfer processes during evaporation in capillary porous structures, Appl. Therm. Eng. 22 (2002) 815–824.
[4] C. Li, G.P. Peterson, Y. Wang, Evaporation/boiling in thin capillary wicks (I) – wick thickness effects, J. Heat Transfer 128 (2006) 1312–1319.
[5] C. Li, G.P. Peterson, Evaporation/boiling in thin capillary wicks (II) – effects of volumetric porosity and mesh size, J. Heat Transfer 128 (2006) 1320–1328.
[6] ESDU, Heat pipes – properties of common small-pore wicks, Data Item No. 79013, Engineering Sciences Data Unit, London, United Kingdom, 1979.